Nuclear Engineering and Technology xxx (xxxx) xxx

Contents lists available at ScienceDirect

Nuclear Engineering and Technology

journal homepage: www.elsevier.com/locate/net

Two-dimensional measurements of the ELM filament using a multi-channel electrical probe array with high time resolution at the far SOL region in the KSTAR

Young-Hun Hong [a], Kwan-Yong Kim [a], Ju-Ho Kim [a], Soo-Hyun Son [b], Hyung-Ho Lee [b], Hyun-Dong Eo [a], Min-Seok Kim [a], Suk-Ho Hong [b], Chin-Wook Chung [a,*]

[a] Department of Electrical Engineering, Hanyang University, 222, Wangsimni-ro, Seongdong-gu, Seoul, 133-791, Republic of Korea
[b] Korea Institute of Fusion Energy (KFE), Daejeon, 34133, Republic of Korea

ARTICLE INFO

Article history:
Received 29 October 2021
Received in revised form
18 March 2022
Accepted 2 May 2022
Available online xxx

Keywords:
Tokamak edge plasma
Two-dimensional electrical diagnostic
ELM behavior
PFC stability
KSTAR

ABSTRACT

For the first time, two-dimensional temporal behavior of the edge localized mode (ELM) filament is measured in the edge tokamak plasma with a multi-channel electrical probe array (MCEP). MCEP, which has 16 floating probes (4 × 4), is mounted at the far scrape-off layer (SOL) region in the KSTAR. An electron temperature and an ion flux are measured by sideband method (SBM), which can achieve two-dimensional measurements with high time resolution. Furthermore, temporal evolutions of the electron temperature and the ion flux are obtained during the ELM occurrence. In the H-mode period, short spikes from ELM bursts are observed in measured plasma parameters, and the trend is similar to that of typical Hα signal. Interestingly, when blob-like ELM filaments crash the probe, the heat flux is significantly higher in a local region of the probe array. The results show that our probe array using the SBM can measure the ELM behavior and the plasma parameters without the effect of the stray current caused by the huge device. This study can provide valuable data needed to understand the interaction between the SOL plasma and the plasma facing components (PFCs).

1. Introduction

In a tokamak plasma, the high confinement mode (H-mode) is characterized by the presence of an edge transport barrier (ETB) resulting in enhanced confinement that is almost twice that of the low confinement mode (L-mode) [1,2]. Thus, it is a promising operation mode for future fusion plasma devices [3]. In H-mode operation, the plasma density and the pressure gradients significantly increase due to the high confinement and stored energy. Furthermore, filamentary perturbations of the plasma density that form along the local magnetic field lines occur frequently in the ETB region (i.e., pedestal) due to instability. Consequently, the edge pedestal structure produces periodic losses of particles and energy from the edge region, i.e., edge-localized mode (ELM) [4–6].

The ELM, first discovered in the ASDEX, is an important phenomenon for the edge plasma in the H-mode operation [2,7]. The filamentary structure of the ELM can be observed and mostly losses to the divertor plate along the magnetic field lines. In addition, the ELM burst leads to a rapid propagation of heat and particles into localized regions of the first wall [8,9]. This propagation can also form a blob structure and is typically observed near the separatrix region, also called the scrape-off layer (SOL) region [10]. These ELM blob and the ELM filament can be extended outward to the SOL region because the confined plasma is typically subjected to radial expansion forces (curvature and $\nabla \mathbf{B}$ forces in toroidal plasmas) [9,11]. Thus, the heat load due to the ELM burst can reach the plasma facing component (PFC) and exceed a tolerance level of typical PFC materials, such as those of the International Thermonuclear Fusion Reactor (ITER) [12]. This indicates that the ELM can cause severe damage and erosion to PFCs of tokamak devices [13–17]. Therefore, it is essential to understand the characteristics of the ELM to improve the lifetime of the fusion device. As a result, many studies have been performed on the characteristics of the ELM and its effects on the boundary plasma in various fusion devices [18–25].

The diagnostics of the tokamak plasma are indispensable for understanding the interaction between the core plasma and the

* Corresponding author.
E-mail address: joykang@hanyang.ac.kr (C.-W. Chung).

https://doi.org/10.1016/j.net.2022.05.003

Please cite this article as: Y.-H. Hong, K.-Y. Kim, J.-H. Kim *et al.*, Two-dimensional measurements of the ELM filament using a multi-channel electrical probe array with high time resolution at the far SOL region in the KSTAR, Nuclear Engineering and Technology, https://doi.org/10.1016/j.net.2022.05.003

PFCs, thus many efforts to diagnose the tokamak plasma have been reported for a stable operation of the fusion device [26–30]. In particular, two-dimensional measurements with high time resolution are required to capture temporal behaviors such as the ELM burst. Thus, several studies have performed diagnostics through two-dimensional optical measurements [10,31–34]. Yun et al. observed the rotating ELM filaments in 2D via an electron cyclotron emission imaging (ECEI) system which has sufficient temporal and spatial resolution [35–38]. A single Langmuir probe measurement, one of the well-known electrical diagnostic methods, can obtain plasma parameters by analyzing the probe current, but it requires time to perform a voltage sweep; high temporal resolution from this measurement is therefore unattainable [39]. A triple probe method, which does not require a voltage sweep, is a suitable diagnostic method for high-resolution measurements [40]. Recently, the time trace and radial profile of the plasma parameters were measured using the triple probe method in the Korea Superconducting Tokamak Advanced Research (KSTAR) [41–44]. Moreover, a floating-type method was developed to measure the temporal behaviors with high time resolution [45–47]. Lee et al. developed the floating harmonic probe (FHP), based on the harmonic method [48]. This probe can get not only the electron temperature but also the ion flux. Recently, a floating harmonic sideband method (SBM) was developed which provides accurate measurements of the plasma parameters even when the measured currents are influenced by considerable stray currents [49,50]. Therefore, SBM is suitable for measuring the tokamak plasma where the cable between the measurement probe and control system is quite long, causing significant stray current [51,52]. However, two-dimensional measurements through the electrical diagnostic method were not performed. Park et al. developed a plasma measurement system applying the sideband method (SBM) that can measure the two-dimensional plasma parameters simultaneously [53]. In this study, SBM was applied to measure the far SOL region of the tokamak plasma, and two-dimensional electrical diagnosis was performed for the first time.

We investigated the two-dimensional spatial evolution of the ELM in the edge tokamak plasma. A multi-channel electrical probe array (MCEP) was mounted on the outboard midplane wall of the KSTAR. The electron temperatures and ion fluxes were obtained by using SBM. In the H-mode period, measured plasma parameters have numerous short spikes that are in good agreement with those of typical Hα signal of the KSTAR. This indicates that the ELM occurrence can be observed using our measurement method. In addition, the spatial evolutions of the electron temperature and the ion flux were measured during the ELM occurrence. Interestingly, experimental results show that there are significant increases in the heat flux at a local region of the probe array when blob-like ELM filaments crash the probe.

2. Experimental setup

2.1. Multi-channel electrical probe array at the far SOL region

The multi-channel electrical probe (MCEP) array, which consists of 16 probes, was used to measure the plasma parameters at the far SOL region in the KSTAR. The far SOL region, represented as being beyond a few centimeters outside the last closed flux surface (LCFS), is characterized by flat profiles of the plasma density [54,55]. Fig. 1(a) shows the components of probe head for MCEP. Each component was modular for easy replacement. The probe head consists of the probe tip, insulating alumina, graphite housing, and signal line. The probe tip was made of cylindrical carbon fiber composite (CFC), which can resist high heat flux without melting, (maximum 1,200°C) and was 12 mm in diameter. The entire tip was covered with an alumina (Silicon nitride, Si_3N_4) tube to insulate it from the outer graphite housing, except for the flat end that serves as the actual probe tip. The distance between adjacent tips is 50 mm. The signal line was covered with a Kapton film which has a high thermal resistance. As shown in Fig. 1(b), the assembled MCEP was composed of 16 probe heads installed on a square plate. To measure the two-dimensional spatial behavior of the ELM filaments at the far SOL region, MCEP was designed in a 4×4 array (0.2×0.2 m^2).

The electron temperature and ion flux at the far SOL region of the KSTAR tokamak plasma was obtained by MCEP. MCEP was mounted on the outboard midplane wall of the KSTAR B-port, as shown in Fig. 2. It was located 125 mm behind the toroidal limiter and 210 mm behind the typical separatrix position of the KSTAR diverted plasmas. The signal lines, which are connected to the measurement control system through a vacuum feed-through, were applied through twisted cable to reduce noise and shielded by a stainless-steel tube (SUS316L) to prevent damage from the tokamak plasma. The coaxial type transmission-line was used for the signal cable outside the tokamak device and total length of the outer cable was about 20 m, which is long enough to generate considerable stray current.

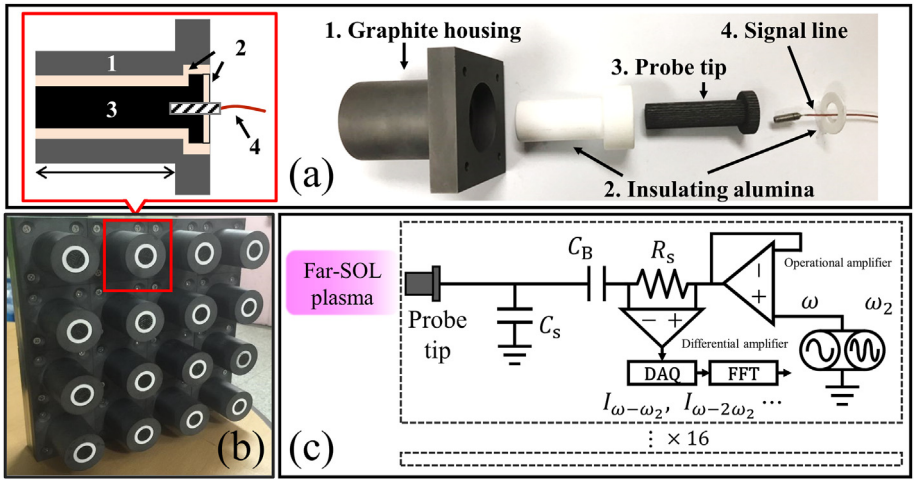

Fig. 1. The multi-channel electrical probe array: (a) components of a probe head for the multi-channel electrical probe array, (b) assembled multi-channel electrical probe array, (c) simultaneous measurement system of the multi-channel electrical probe array.

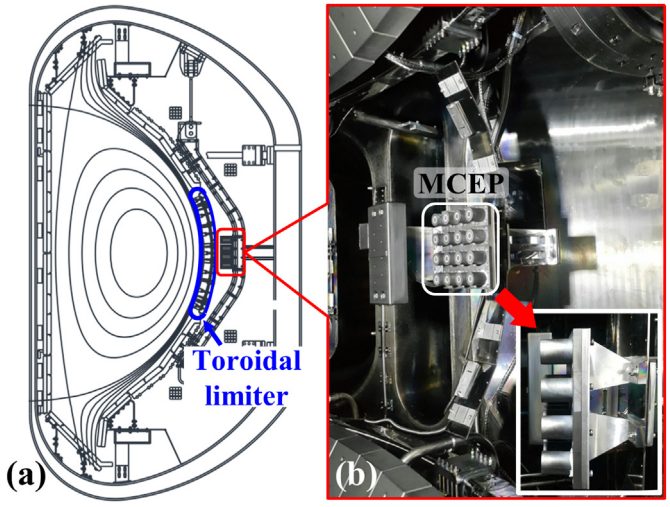

Fig. 2. View of the multi-channel electrical probe array in the KSTAR: (a) poloidal cross-sectional view of the tokamak device, (b) the multi-channel electrical probe array mounted in the B-port of the KSTAR.

The measurement control system was composed of a data acquisition system (DAQ) and a driving circuit board, as shown in Fig. 1(c). Two amplifiers were used, one for buffer and one for sensing voltage. The model of DAQ is PXIe-6358 (National Instruments, NI), which has 16 simultaneous analog inputs with a 1.25 MHz sampling rate for each channel, and it was mounted on the PXI Express Chassis (NI, model: PXIe-1073).

2.2. Principles of the measurement

All measurements were recorded as raw data and analyzed by post-processing method which is effective to obtain high time resolution [51]. The number of data points measured in 1 s is 1,250,000 because the sampling rate of DAQ is 1.25 MHz. The time resolution is determined by the number of data points: 1 ms is the time resolution for 1,250 data points. In addition, the time resolution was enhanced by selecting the frequency of applied voltage and the number of data points. When the frequency of 125 kHz was selected for the applied voltage, 10 data points (1 period of the 125 kHz at the sampling rate of 1.25 MHz) are analyzed for the time resolution of 8 μs at our DAQ. But high signal-to-noise ratio is necessary for reasonable measurement because random noise increases as the number of data points decreases. Here, the time resolution is 200 μs for each channel and that resolution yields an appropriate signal-to-noise ratio (SNR). In this study, all measurement data were recorded at 12 s.

After we analyzed by post-processing, the electron temperature and ion flux were obtained by applying the sideband method (SBM) [49,50]. The SBM that can measure plasma parameters such as the electron temperature and ion flux is an application of the floating harmonics probe developed by Lee et al. [48]. The sinusoidal AC voltage, $v_0[\cos(\omega t)+\cos(\omega_2 t)]$, was applied to each probe tip from the circuit board. Here, the applied AC signal frequency (ω, ω_2) was, respectively, 125 kHz and 25 kHz, and the applied AC voltage (v_0) was 3 V. The SBM assumes that the electrons are in a Maxwellian distribution, and with this assumption, the electron temperature (T_e) and the ion flux (Γ_i) are obtained as follows:

$$T_e \approx \frac{v_0}{4}\frac{I_{\omega\pm\omega_2}}{I_{\omega\pm2\omega_2}}\left(\frac{v_0}{T_e}<1\right) \quad (1)$$

$$\Gamma_i = \frac{I_{\omega\pm\omega_2}}{2(0.49eA_p)}\left[\frac{I_0(v_0/T_e)}{I_1(v_0/T_e)}\right]^2, \quad (2)$$

where $I_{\omega\pm\omega_2}$, $I_{\omega\pm2\omega_2}$, I_0, I_1, e, and A_p are the first and second intermodulation frequency currents the zero- and first-order modified Bessel functions, the electron charge, and the area of the probe, respectively. Note that the Bohm velocity is not needed to determine the ion flux in this method [48,49]. The AC signal voltage was applied near the floating potential where the electron and ion currents are equal because the blocking capacitor ($C_B = 100\ \mu F$) was connected in series with the probe tip. The ion flux, Γ_i, is collected by the flat probe tips almost perpendicular to the magnetic field. Thus, a parallel ion flux ($\Gamma_{i,\parallel}$) can be expressed as $\Gamma_i = \Gamma_{i,\parallel}\sin\theta$, where $\theta \approx 5^\circ$ is the angle between the magnetic field line and the surface of the probe tip. In huge plasma facilities such as tokamak devices, typical electrical measurements can be affected by large stray currents due to the stray capacitance in long and dense measurement cables. However, the intermodulation frequency currents are not influenced by the stray current, because the intermodulation current is generated by the nonlinearity of the plasma sheath rather than by stray capacitance of the measurement system. Moreover, there is numerous fluctuations in various frequency bands and these fluctuations can cause the interference in the measurements. In SBM, the plasma parameters are obtained from the selected frequency combination among the various frequency combinations (e.g., $I_{\omega-\omega_2}$ & $I_{\omega-2\omega_2}$, $I_{\omega+\omega_2}$ & $I_{\omega+2\omega_2}$, and $I_{\omega+2\omega_2}$ & $I_{2\omega}$). Among these combinations, we can choose the frequency combination with the least fluctuation. Here, the combination of $I_{\omega-\omega_2}$ and $I_{\omega-2\omega_2}$ was selected. Thus, SBM is very useful when the measured currents are influenced by the considerable stray currents and the fluctuations in various frequency bands generated in the system [51,52].

In this paper, the modified Shepard method was applied, which is a suitable interpolation for constructing the two-dimensional distribution of the plasma parameters [56,57]. The two-dimensional measurement can be achieved through a combination of various features of our diagnostic method: the floating harmonic probe (FHP) method that allows real-time measurement of T_e and Γ_i without the voltage sweep, the SBM that can provide accurate measurements of the plasma parameters even when affected by stray currents, and the post-processing method which is effective to obtain high time resolution.

3. Results and discussion

Fig. 3 shows time traces of NBI heating powers, electron line densities, and Hα signal intensities in the discharge No. 18847 of the KSTAR. The plasma was mainly heated by NBI (neutral beam injection) in the KSTAR. The experimental conditions in the discharge No. 18847 are as follows: toroidal magnetic field, $B_T = 1.8$ T; plasma current, $I_p = 600$ kA. The NBI power (P_{NBI}) is about 1.7 MW from 2 s to 6 s and about 4 MW from 6 s to 16 s. There are three regimes in the duration of the measurement: initial regime (0–2 s), low P_{NBI} regime (2–6 s), and high P_{NBI} regime (6–16 s). The line-averaged electron density, n_e, are shown in Fig. 3(b). n_e measured with millimeter-wave interferometer [58] represents plasma density in the entire region of the tokamak plasma.

Hα signal is measured by Hα monitor arrays [59]. Numerous short spikes of Hα signal ($\lambda = 656$ nm) are observed after the NBI heating power is applied, as shown in Fig. 3(c). These spikes indicate that the edge-localized mode (ELM) occurred in the edge tokamak plasma and the plasma is in the ELMy H-mode operation.

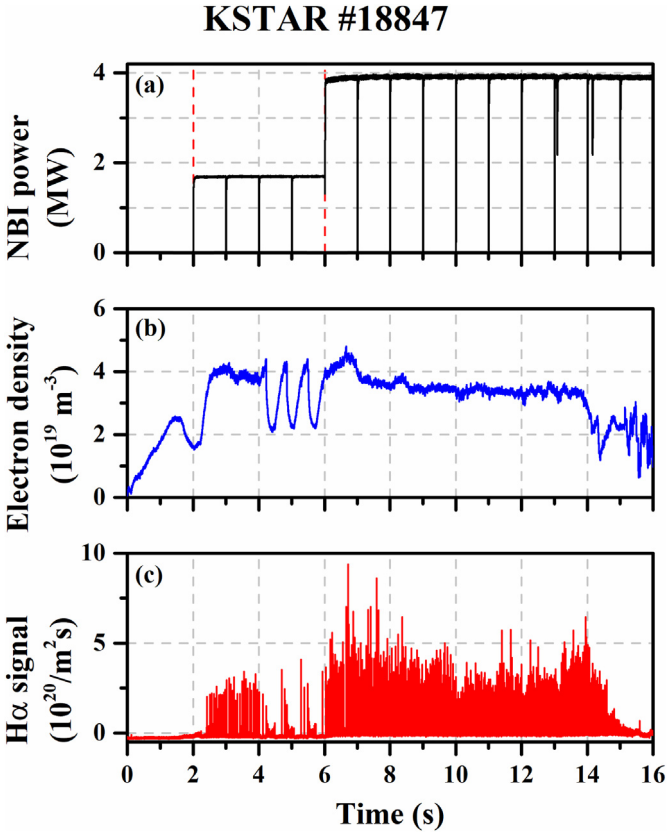

Fig. 3. Typical time traces of several plasma parameters in discharge No. 18847 of the KSTAR. (a) NBI heating power, (b) line-averaged electron density, (c) Hα signal.

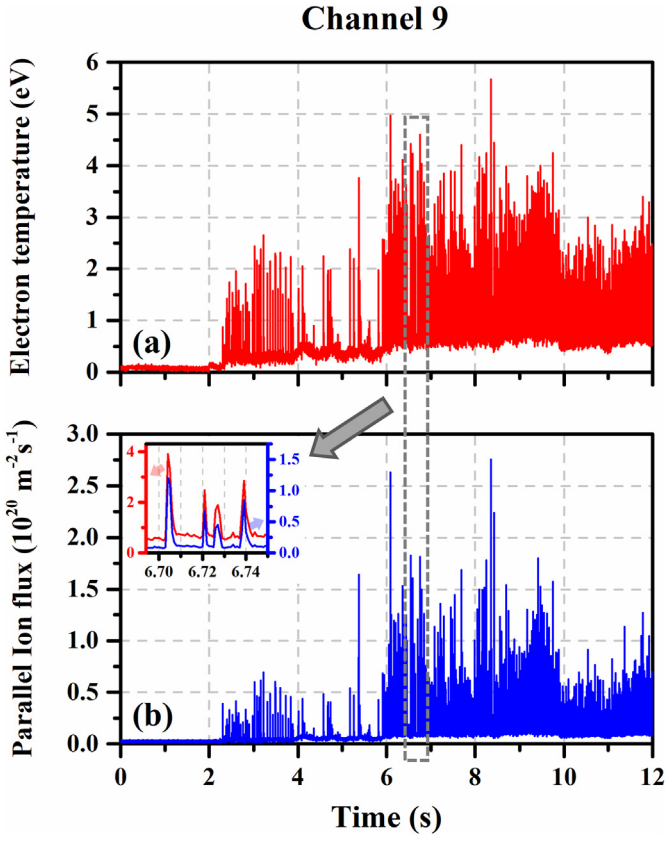

Fig. 4. Time traces of measured plasma parameters in the far SOL region of channel 9 in discharge No. 18847 of the KSTAR: (a) electron temperature and (b) parallel ion flux.

The frequency of the ELM occurrence can be obtained by counting these spikes. The frequency of the ELM occurrence increases by about 4.6 times in the high P_{NBI} region than in the low P_{NBI} region. Moreover, the intensity of the Hα signal spike increased by about 1.3 times.

Fig. 4 shows time traces of the electron temperature (T_e) and the parallel ion flux ($\Gamma_{i,\parallel}$) at the far SOL region as measured by MCEP. In enlarged view of Fig. 4(b), T_e and $\Gamma_{i,\parallel}$ from 6.69 s to 6.75 s are also presented to verify that the events are synchronized. Since the background T_e and $\Gamma_{i,\parallel}$ are much lower than those from the ELM filament, the ELM occurrence is distinctly observed by the measured parameters. T_e of about 1.4–4 eV and $\Gamma_{i,\parallel}$ of about 8×10^{19} m^{-2}s^{-1} were obtained when the ELM occurred. T_e and $\Gamma_{i,\parallel}$ are compared to those measured by the triple probe under almost similar experimental conditions [41–44]. T_e and $\Gamma_{i,\parallel}$ measured by the triple probe were slightly higher than our results; T_e was up to about 40 eV and $\Gamma_{i,\parallel}$ was about $10^{20} - 10^{21}$ m^{-2}s^{-1} when the ELM occurred. This difference is because MCEP was installed about 50–100 mm behind the triple probe, resulting in a slightly lower value.

Note that short spikes of T_e are observed during the H-mode operation, and these values are about 1.4 times higher in the high P_{NBI} regime. The trend of T_e is in good agreement with that of Hα signal, as can be seen in Fig. 3(c). This can be understood in that when the ELM occurs, the ELM filament crashed to MCEP and a short spike of T_e is observed at the same time. By counting the spikes of T_e, the ELM occurs about 4.9 times more frequently in the high P_{NBI} regime than in the low P_{NBI} regime. The fact that the ELM occurs more frequently in the high P_{NBI} regime is consistent with the characteristics of type I ELM [60].

In Fig. 4(b), $\Gamma_{i,\parallel}$ also has a similar trend; numerous short spikes are observed, and the value of $\Gamma_{i,\parallel}$ and the frequency of the ELM occurrence are different depending on the period of the discharge (low P_{NBI} regime and high P_{NBI} regime). Furthermore, the spike values of $\Gamma_{i,\parallel}$ also increase by about 1.7 times. These imply that as the applied P_{NBI} increases, the ELM occurs more frequently and the strength of the ELM, i.e., the energy loss, also increases.

To understand the temporal behavior of these ELM filaments, measured T_e and Γ_i are imaged in 2D. Fig. 5 shows the two-dimensional spatial evolution of T_e and Γ_i measured by MCEP. The analysis time resolution is 200 μs, and the period is about 6.703–6.706 s (see enlarged view of Fig. 4(b)). The position of each probe channel is marked in 3,000 μs of Fig. 5(a).

At 200 μs, the measured T_e is relatively high in channels 10 and 14. Moreover, the high T_e is measured in channel 1 at 400 μs and then the spatial distribution of T_e is almost uniform up to 800 μs. Interestingly, T_e has a lower value first on the right side with increasing time-step. The distribution of Γ_i is consistent with that of T_e, as shown in Fig. 5(b). The spatial evolution of the plasma parameters at 200 μs can be understood as the behavior of the expanding ELM filament. Since the confined plasma is generally subjected to radial expansion forces, the ELM filament can be extended outward to the LCFS. Thus, not only the radially propagated blob-like ELM filament, but also the ELM filament can be measured when the filamentary structures are extended to the probe array in the far SOL region. The expanded ELM filament temporarily reaches a local region of the probe array, resulting in a sharp increase in the plasma parameters of the corresponding channel and this increment vanishes almost immediately as time passes.

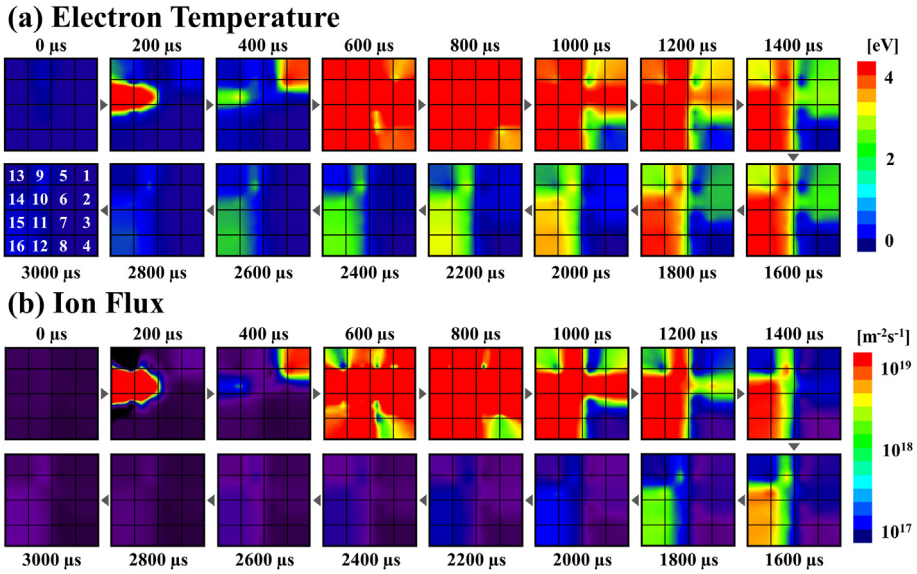

Fig. 5. Two-dimensional (a) electron temperature and (b) ion flux measured by MCEP.

On the other hand, the spatial evolution of the plasma parameters from 400 μs to 2,000 μs shows a different trend from that of 200 μs. This spatial evolution at this period seems to be that the blob-like ELM filament crashes and escapes the probe array. When the ELM filaments burst, the filament can escape from the confinement in form of a blob [61]. It can be predicted that the blob-like ELM filament covers the entire probe array and exits to the left side. This may indicate that the blob-like ELM filament that collides with the divertor or the wall can flow along their surface rather than transferring energy to the target and disappearing. It is also noted that the blob-like ELM filament seems to exit downwards. In the KSTAR, the rotation of the ELM filaments generally is counterclockwise (electron diamagnetic drift direction) in the poloidal cross-sectional view of Fig. 2(a) [36,37]. This suggests that the radial propagation direction of the ELM blobs is independent or less dependent on the direction of the ELM filaments.

The heat flux is a crucial factor for consideration to stably operate the ELMy H-mode. The parallel heat flux at the sheath edge, $q_{\parallel,se}$, can be derived using the following equation:

$$q_{\parallel,se} = \gamma e T_e \Gamma_{i,\parallel}, \tag{3}$$

where e is the electron charge and γ is the sheath transmission coefficient as given in $\gamma = 7$ [43,62,63]. During the ELM burst, $q_{\parallel,se}$ of about 10 kW/m^2 is obtained at the far SOL region. As mentioned above, the spike value of T_e and $\Gamma_{i,\parallel}$ increased at the high P_{NBI} regime. Since $q_{\parallel,se}$ is proportional to both T_e and $\Gamma_{i,\parallel}$, thus it is approximately doubled at the high P_{NBI} regime. In general, about 20–30% of the power applied to the plasma is radiated and lost to the first wall. Thus, the effect of the heat flux by the ELM burst on the PFCs is negligible compared to the radiated energy flux in the KSTAR. Nevertheless, it should be noted that at 200 μs, the heat flux of channel 14 is about 10^2 times higher than that of channel 8. This implies that the heat flux is concentrated in the local region, as can be inferred from Fig. 5. In practice, the averaged heat flux at 200 μs is only 8 kW/m^2 while the heat flux of channel 14 is 35 kW/m^2. Therefore, even though the heat flux per unit area under these experimental conditions is not critical enough to damage the walls or divertors, the investigation of these concentrated heat fluxes would be necessary for larger fusion devices, such as DEMO (demonstration power plant) and ITER.

In future work, we will improve the time and spatial resolution of MCEP to observe the behavior of the ELM more precisely and will measure the tokamak plasma in the divertor region of the KSTAR by installing the enhanced MCEP. Furthermore, the valuable data needed to understand the interaction between the edge plasma and the PFC can be obtained by installing MCEP in critical region of PFCs.

4. Conclusion

In this study, the temporal behaviors of the ELM are measured by MCEP in the KSTAR tokamak plasma for the first time as electrical probe diagnostics. The plasma parameters (T_e, $\Gamma_{i,\parallel}$) are obtained by using SBM with high time resolution (200 μs) at the far SOL region. In the H-mode period, numerous short spikes in the electron temperature as well as in the ion flux are observed, and the trend is consistent with typical Hα signal of the KSTAR. These spikes are caused by the ELM occurrences which are characterized by periodic losses of particles and energy from the SOL region. When the ELM occurs, the measured electron temperature is about 1.4–4 eV and the parallel ion flux is about 8×10^{19} m^{-2}s^{-1}. Note that the ELM occurs about 4.9 times more frequently in the high P_{NBI} regime than in the low P_{NBI} regime. This is consistent with the characteristics of type I ELM.

Through the two-dimensional measurements and interpolation of the plasma parameters, the spatial evolution is obtained. The radially propagated blob-like ELM filament as well as the extended ELM filament is observed in 2D. When the blob-like ELM filaments crash the probe, the parallel heat flux, $q_{\parallel,se}$, obtained from the measured plasma parameters is significantly higher in the local region of the probe array. This indicates that the heat flux from the ELM burst is concentrated in the local region. These concentrated heat fluxes can damage the first walls for larger fusion devices where the applied power is much higher such as DEMO and ITER. Therefore, the results show that our method for the far SOL region diagnostics can give useful data such as the plasma parameters and the ELM behaviors needed to understand the interaction between the edge tokamak plasma and the PFCs.

Declaration of competing interest

The authors declare that they have no known competing financial interests or personal relationships that could have appeared to influence the work reported in this paper.

Acknowledgment

This work was supported by the National Research Foundation of Korea (NRF-2019M1A7A1A03087579, NRF-2021R1I1A 1A01050312), the Ministry of Trade, Industry and Energy (20011226, 20009415, 20010412, 20012609).

Appendix A. Supplementary data

Supplementary data to this article can be found online at https://doi.org/10.1016/j.net.2022.05.003.

References

[1] K. Toi, F. Watanabe, S. Ohdachi, S. Morita, X. Gao, K. Narihara, S. Sakakibara, K. Tanaka, T. Tokuzawa, H. Urano, LH transition and edge transport barrier formation on LHD, Fusion Sci. Technol. 58 (2010) 61–69, https://doi.org/10.13182/FST10-A10794.

[2] F. Wagner, G. Becker, K. Behringer, D. Campbell, A. Eberhagen, W. Engelhardt, G. Fussmann, O. Gehre, J. Gernhardt, G.v. Gierke, Regime of improved confinement and high beta in neutral-beam-heated divertor discharges of the ASDEX tokamak, Phys. Rev. Lett. 49 (1982) 1408, https://doi.org/10.1103/PhysRevLett.49.1408.

[3] F. Wagner, A quarter-century of H-mode studies, Plasma Phys. Contr. Fusion 49 (2007) B1, https://doi.org/10.1088/0741-3335/49/12B/S01.

[4] H. Zohm, Edge localized modes (ELMs), Plasma Phys. Contr. Fusion 38 (1996) 105, https://doi.org/10.1088/0741-3335/38/2/001.

[5] J. Connor, A review of models for ELMs, Plasma Phys. Contr. Fusion 40 (1998) 191, https://doi.org/10.1088/0741-3335/40/2/003.

[6] L. Vinet, A. Zhedanov, A 'missing'family of classical orthogonal polynomials, J. Phys. Math. Theor. 44 (2011), 085201, https://doi.org/10.1088/1751-8113/44/8/085201.

[7] M. Keilhacker, G. Becker, K. Bernhardi, A. Eberhagen, M. Elshaer, O. Gehre, J. Gernhardt, E. Glock, G. Haas, F. Karger, S. Kissel, O. Kluber, M. Kornherr, K. Lackner, G. Lisitano, G.G. Lister, J. Massig, H.M. Mayer, K. Mccormick, D. Meisel, E. Meservey, E.R. Muller, H. Murmann, H. Niedermeyer, W. Poschenrieder, H. Rapp, B. Richter, H. Rohr, F. Ryter, F. Schneider, G. Siller, P. Smeulders, F. Soldner, E. Speth, A. Stabler, K. Steinmetz, K.H. Steuer, Z. Szymanski, G. Venus, O. Vollmer, F. Wagner, G. Fussman, G. Vongierke, Confinement studies in L-type and H-type Asdex discharges, Plasma Phys. Contr. Fusion 26 (1984) 49–63, https://doi.org/10.1088/0741-3335/26/1A/305.

[8] J.R. Myra, D.A. D'Ippolito, D.P. Stotler, S.J. Zweben, B.P. LeBlanc, J.E. Menard, R.J. Maqueda, J. Boedo, Blob birth and transport in the tokamak edge plasma: analysis of imaging data, Phys. Plasmas 13 (2006), 092509, https://doi.org/10.1063/1.2355668.

[9] D.A. D'ippolito, J.R. Myra, S.J. Zweben, Convective transport by intermittent blob-filaments: comparison of theory and experiment, Phys. Plasmas 18 (2011), 060501, https://doi.org/10.1063/1.3594609.

[10] J.A. Alonso, P. Andrew, A. Neto, J.L. de Pablos, E. de la Cal, H. Fernandes, W. Fundamenski, C. Hidalgo, G. Kocsis, A. Murari, G. Petravich, R.A. Pitts, L. Rios, C. Silva, E.-J. Contributors, Fast visible imaging of ELM-wall interactions on JET, J. Nucl. Mater. 390–91 (2009) 797–800, https://doi.org/10.1016/j.jnucmat.2009.01.211.

[11] S.I. Krasheninnikov, On scrape off layer plasma transport, Phys. Lett. 283 (2001) 368–370, https://doi.org/10.1016/S0375-9601(01)00252-3.

[12] A.S. Kukushkin, H.D. Pacher, G. Federici, G. Janeschitz, A. Loarte, G.W. Pacher, Divertor issues on ITER and extrapolation to reactors, Fusion Eng. Des. 65 (2003) 355–366, https://doi.org/10.1016/S0920-3796(02)00380-0.

[13] D.N. Hill, A review of ELMs in divertor tokamaks, J. Nucl. Mater. 241 (1997) 182–198, https://doi.org/10.1016/S0022-3115(97)80039-6.

[14] A. Loarte, G. Saibene, R. Sartori, D. Campbell, M. Becoulet, L. Horton, T. Eich, A. Herrmann, G. Matthews, N. Asakura, A. Chankin, A. Leonard, G. Porter, G. Federici, G. Janeschitz, M. Shimada, M. Sugihara, Characteristics of type I ELM energy and particle losses in existing devices and their extrapolation to ITER, Plasma Phys. Contr. Fusion 45 (2003) 1549–1569, https://doi.org/10.1088/0741-3335/45/9/302.

[15] G. Federici, A. Loarte, G. Strohmayer, Assessment of erosion of the ITER divertor targets during type I ELMs, Plasma Phys. Contr. Fusion 45 (2003) 1523–1547, https://doi.org/10.1088/0741-3335/45/9/301.

[16] B.N. Bazylev, Y. Koza, I.S. Landman, J. Linke, S.E. Pestchanyi, H. Wuerz, Energy threshold of brittle destruction for carbon-based materials, Phys. Scripta T111 (2004) 213–217, https://doi.org/10.1238/Physica.Topical.111a00213.

[17] W. Fundamenski, R. Pitts, A model of ELM filament energy evolution due to parallel losses, Plasma Phys. Contr. Fusion 48 (2005) 109, https://doi.org/10.1088/0741-3335/48/1/008.

[18] H.W. Muller, J. Adamek, R. Cavazzana, G.D. Conway, C. Fuchs, J.P. Gunn, A. Herrmann, J. Horacek, C. Ionita, A. Kallenbach, M. Kocan, M. Maraschek, C. Maszl, F. Mehlmann, B. Nold, M. Peterka, V. Rohde, J. Schweinzer, R. Schrittwieser, N. Vianello, E. Wolfrum, M. Zuin, A.U. Team, Latest investigations on fluctuations, ELM filaments and turbulent transport in the SOL of ASDEX Upgrade, Nucl. Fusion 51 (2011), 073023, https://doi.org/10.1088/0029-5515/51/7/073023.

[19] D.L. Rudakov, J.A. Boedo, R.A. Moyer, P.C. Stangeby, J.G. Watkins, D.G. Whyte, L. Zeng, N.H. Brooks, R.P. Doerner, T.E. Evans, M.E. Fenstermacher, M. Groth, E.M. Hollmann, S.I. Krasheninnikov, C.J. Lasnier, A.W. Leonard, M.A. Mahdavi, G.R. McKee, A.G. McLean, A.Y. Pigarov, W.R. Wampler, G. Wang, W.P. West, C.P.C. Wong, Far SOL transport and main wall plasma interaction in DIII-D, Nucl. Fusion 45 (2005) 1589–1599, https://doi.org/10.1088/0029-5515/45/12/014.

[20] R.A. Pitts, P. Andrew, G. Arnoux, T. Eich, W. Fundamenski, A. Huber, C. Silva, D. Tskhakaya, J.E. Contributors, ELM transport in the JET scrape-off layer, Nucl. Fusion 47 (2007) 1437–1448, https://doi.org/10.1088/0029-5515/47/11/005.

[21] N. Oyama, Y. Sakamoto, A. Isayama, M. Takechi, P. Gohil, L.L. Lao, P.B. Snyder, T. Fujita, S. Ide, Y. Kamada, Y. Miura, T. Oikawa, T. Suzuki, H. Takenaga, K. Toi, J. Team, Energy loss for grassy ELMs and effects of plasma rotation on the ELM characteristics in JT-60U, Nucl. Fusion 45 (2005) 871–881, https://doi.org/10.1088/0029-5515/45/8/014.

[22] J.W. Ahn, H.S. Kim, Y.S. Park, L. Terzolo, W.H. Ko, J.K. Park, A.C. England, S.W. Yoon, Y.M. Jeon, S.A. Sabbagh, Y.S. Bae, J.G. Bak, S.H. Hahn, D.L. Hillis, J. Kim, W.C. Kim, J.G. Kwak, K.D. Lee, Y.S. Na, Y.U. Nam, Y.K. Oh, S.I. Park, Confinement and ELM characteristics of H-mode plasmas in KSTAR, Nucl. Fusion 52 (2012), 114001, https://doi.org/10.1088/0029-5515/52/11/114001.

[23] A. Degeling, Y. Martin, J. Lister, L. Villard, V. Dokouka, V. Lukash, R. Khayrutdinov, Magnetic triggering of ELMs in TCV, Plasma Phys. Contr. Fusion 45 (2003) 1637, https://doi.org/10.1088/0741-3335/45/9/306.

[24] N. Hayashi, T. Takizuka, N. Aiba, N. Oyama, T. Ozeki, S. Wiesen, V. Parail, Integrated simulation of ELM energy loss and cycle in improved H-mode plasmas, Nucl. Fusion 49 (2009), 095015, https://doi.org/10.1088/0029-5515/49/9/095015.

[25] A. Kojima, N. Oyama, Y. Sakamoto, Y. Kamada, H. Urano, K. Kamiya, T. Fujita, H. Kubo, N. Aiba, Fast dynamics of type I and grassy ELMs in JT-60U, Nucl. Fusion 49 (2009), 115008, https://doi.org/10.1088/0029-5515/49/11/115008.

[26] M. Bornatici, R. Cano, O. Debarbieri, F. Engelmann, Electron-cyclotron emission and absorption in fusion plasmas, Nucl. Fusion 23 (1983) 1153–1257, https://doi.org/10.1088/0029-5515/23/9/005.

[27] I.H. Hutchinson, Principles of plasma diagnostics, Plasma Phys. Contr. Fusion 44 (2002) 2603, https://doi.org/10.1088/0741-3335/44/12/701.

[28] B. Lloyd, J.W. Ahn, R.J. Akers, L.C. Appel, E.R. Arends, K.B. Axon, R.J. Buttery, C. Byrom, P.G. Carolan, C. Challis, D. Ciric, N.J. Conway, M. Cox, G.F. Counsell, G. Cunningham, A. Darke, A. Dnestrovskij, J. Dowling, M.R. Dunstan, A.R. Field, S.J. Fielding, S. Gee, M.P. Gryaznevich, P. Helander, M. Hole, M.B. Hood, P.A. Jones, A. Kirk, I.P. Lehane, G.P. Maddison, S.J. Manhood, R. Martin, G.J. McArdle, K.G. McClements, M.A. McGrath, H. Meyer, A.W. Morris, S.K. Nielsen, M. Nightingale, A. Patel, T. Pinfold, M.N. Price, J. Qin, C. Ribeiro, C.M. Roach, D.C. Robinson, O. Sauter, V. Shevchenko, S. Shibaev, K. Stammers, A. Sykes, A. Tabasso, D. Taylor, M.R. Tournianski, G. Turri, M. Valovic, G. Voss, M.J. Walsh, S. Warder, J.R. Watkins, H.R. Wilson, Y. Yang, S. You, Overview of recent experimental results on MAST, Nucl. Fusion 43 (2003) 1665–1673, https://doi.org/10.1088/0029-5515/43/12/012.

[29] A. Kirk, T. Eich, A. Herrmann, H.W. Muller, L.D. Horton, G.F. Counsell, M. Price, V. Rohde, V. Bobkov, B. Kurzan, J. Neuhauser, H. Wilson, A.U.a.M. Teams, The spatial structure of type-I ELMs at the mid-plane in ASDEX Upgrade and a comparison with data from MAST, Plasma Phys. Contr. Fusion 47 (2005) 995–1013, https://doi.org/10.1088/0741-3335/47/7/003.

[30] A. Kirk, B. Koch, R. Scannell, H.R. Wilson, G. Counsell, J. Dowling, A. Herrmann, R. Martin, M. Walsh, M. team, Evolution of filament structures during edge-localized modes in the MAST Tokamak, Phys. Rev. Lett. 96 (2006), 185001, https://doi.org/10.1103/PhysRevLett.96.185001.

[31] J.H. Yu, D.L. Rudakov, A.Y. Pigarov, R.D. Smirnov, N.H. Brooks, S.H. Muller, W.P. West, Fast camera imaging of dust in the DIII-D tokamak, J. Nucl. Mater. 390–91 (2009) 216–219, https://doi.org/10.1016/j.jnucmat.2009.01.053.

[32] S. von Goeler, W. Stodiek, N. Sauthoff, Studies of internal disruptions and m= 1 oscillations in tokamak discharges with soft—x-ray techniques, Phys. Rev. Lett. 33 (1974) 1201, https://doi.org/10.1103/PhysRevLett.33.1201.

[33] I.G.J. Classen, J.E. Boom, W. Suttrop, E. Schmid, B. Tobias, C.W. Domier, N.C. Luhmann, A.J.H. Donne, R.J.E. Jaspers, P.C. de Vries, H.K. Park, T. Munsat, M. Garcia-Munoz, P.A. Schneider, 2D electron cyclotron emission imaging at ASDEX Upgrade (invited), Rev. Sci. Instrum. 81 (2010), 10D929, https://doi.org/10.1063/1.3483214.

[34] B. Tobias, C.W. Domier, T. Liang, X. Kong, L. Yu, G.S. Yun, H.K. Park, I.G. Classen, J.E. Boom, A.J. Donne, T. Munsat, R. Nazikian, M. Van Zeeland, R.L. Boivin, N.C. Luhmann Jr., Commissioning of electron cyclotron emission imaging instrument on the DIII-D tokamak and first data, Rev. Sci. Instrum. 81 (2010), 10D928, https://doi.org/10.1063/1.3460456.

[35] G.S. Yun, W. Lee, M.J. Choi, J.B. Kim, H.K. Park, C.W. Domier, B. Tobias, T. Liang, X. Kong, N.C. Luhmann Jr., A.J. Donne, Development of KSTAR ECE imaging system for measurement of temperature fluctuations and edge density

fluctuations, Rev. Sci. Instrum. 81 (2010), 10D930, https://doi.org/10.1063/1.3483209.
[36] G.S. Yun, W. Lee, M.J. Choi, J. Lee, H.K. Park, B. Tobias, C.W. Domier, N.C. Luhmann Jr., A.J. Donne, J.H. Lee, K. Team, Two-dimensional visualization of growth and burst of the edge-localized filaments in KSTAR H-mode plasmas, Phys. Rev. Lett. 107 (2011), 045004, https://doi.org/10.1103/PhysRevLett.107.045004.
[37] G. Yun, W. Lee, M. Choi, J. Lee, H. Park, C. Domier, N. Luhmann Jr., B. Tobias, A. Donné, J. Lee, Two-dimensional imaging of edge-localized modes in KSTAR plasmas unperturbed and perturbed by n= 1 external magnetic fields, Phys. Plasmas 19 (2012), 056114, https://doi.org/10.1063/1.3694842.
[38] G.S. Yun, W. Lee, M.J. Choi, J. Lee, M. Kim, J. Leem, Y. Nam, G.H. Choe, H.K. Park, H. Park, D.S. Woo, K.W. Kim, C.W. Domier, N.C. Luhmann Jr., N. Ito, A. Mase, S.G. Lee, Quasi 3D ECE imaging system for study of MHD instabilities in KSTAR, Rev. Sci. Instrum. 85 (2014), 11D820, https://doi.org/10.1063/1.4890401.
[39] M.A. Lieberman, A.J. Lichtenberg, Principles of Plasma Discharges and Materials Processing, John Wiley & Sons, 2005.
[40] S.L. Chen, T. Sekiguchi, Instantaneous direct-display system of plasma parameters by means of triple probe, J. Appl. Phys. 36 (1965) 2363–2375, https://doi.org/10.1063/1.1714492.
[41] J. Bak, Y. Oh, H. Kim, S. Hahn, S. Yoon, Y. Jeon, W. Xiao, W. Ko, W. Kim, J. Kwak, Electric probe measurements at edge region during H-mode discharges in KSTAR, Contrib. Plasma Phys. 53 (2013) 69–74, https://doi.org/10.1002/ctpp.201310012.
[42] J. Bak, H. Kim, M. Bae, J. Juhn, D. Seo, E. Bang, S. Shim, K. Chung, H. Lee, S. Hong, Investigation of SOL parameters and divertor particle flux from electric probe measurements in KSTAR, J. Nucl. Mater. 463 (2015) 424–427, https://doi.org/10.1016/j.jnucmat.2014.11.075.
[43] H.S. Kim, J.G. Bak, M.K. Bae, K.S. Chung, S.H. Hong, Electric probe diagnostics for measuring SOL parameters, wall and divertor fluxes in KSTAR, Fusion Eng. Des. 109 (2016) 809–816, https://doi.org/10.1016/j.fusengdes.2016.01.070.
[44] M.-K. Bae, R. Pitts, J. Bak, S.-H. Hong, H. Kim, H. Lee, I. Kang, K.-S. Chung, Type I ELM filament heat fluxes on the KSTAR main chamber wall, Nucl. Mater. Energy 12 (2017) 1259–1264, https://doi.org/10.1016/j.nme.2017.04.006.
[45] R. Van Nieuwenhove, G. Van Oost, Novel Langmuir probe technique for the real-time measurement of the electron temperature, Rev. Sci. Instrum. 59 (1988) 1053–1056, https://doi.org/10.1063/1.1139724.
[46] J.A. Boedo, D. Gray, R.W. Conn, P. Luong, M. Schaffer, R.S. Ivanov, A.V. Chernilevsky, G. Van Oost, T. Team, On the harmonic technique to measure electron temperature with high time resolution, Rev. Sci. Instrum. 70 (1999) 2997–3006, https://doi.org/10.1063/1.1149888.
[47] D.L. Rudakov, J.A. Boedo, R.A. Moyer, R.D. Lehmer, G. Gunner, J.G. Watkins, Fast electron temperature diagnostic based on Langmuir probe current harmonic detection on DIII-D, Rev. Sci. Instrum. 72 (2001) 453–456, https://doi.org/10.1063/1.1310577.
[48] M.H. Lee, S.H. Jang, C.W. Chung, Floating probe for electron temperature and ion density measurement applicable to processing plasmas, J. Appl. Phys. 101 (2007), 033305, https://doi.org/10.1063/1.2204352.
[49] S.H. Jang, G.H. Kim, C.W. Chung, Harmonic analysis of sideband signals generated in plasmas, Thin Solid Films 519 (2011) 7042–7044, https://doi.org/10.1016/j.tsf.2011.04.132.
[50] D.H. Kim, H.C. Lee, Y.S. Kim, C.W. Chung, Plasma diagnostic method using intermodulation frequencies in a Langmuir probe, Appl. Phys. Lett. 103 (2013), 084103, https://doi.org/10.1063/1.4818822.
[51] D.H. Kim, S.H. Hong, I.S. Park, H.C. Lee, H.J. Kang, C.W. Chung, Probe diagnostics in the far scrape-off layer plasma of Korea Superconducting Tokamak Advanced Research tokamak using a sideband harmonic method, Rev. Sci. Instrum. 86 (2015), 123508, https://doi.org/10.1063/1.4937610.
[52] K.-Y. Kim, S.-H. Son, S.-H. Hong, I.-S. Park, J.-H. Kim, J.-w. Lee, C.-W. Chung, Simultaneous measurements of plasma parameters and blob characteristics at the far-SOL region using a hybrid probe in KSTAR, Fusion Eng. Des. 172 (2021), 112900, https://doi.org/10.1016/j.fusengdes.2021.112900.
[53] I.S. Park, D.H. Kim, K.H. Kim, C.W. Chung, Temporal evolution of two-dimensional electron temperature and ion flux on a substrate in a pulsed-power inductively coupled plasma, Phys. Plasmas 24 (2017), 053510, https://doi.org/10.1063/1.4982815.
[54] B.A. Carreras, V.E. Lynch, B. LaBombard, Structure and properties of the electrostatic fluctuations in the far scrape-off layer region of Alcator C-Mod, Phys. Plasmas 8 (2001) 3702–3707, https://doi.org/10.1063/1.1387266.
[55] B. LaBombard, R.L. Boivin, M. Greenwald, J. Hughes, B. Lipschultz, D. Mossessian, C.S. Pitcher, J.L. Terry, S.J. Zweben, A. Grp, Particle transport in the scrape-off layer and its relationship to discharge density limit in Alcator C-Mod, Phys. Plasmas 8 (2001) 2107–2117, https://doi.org/10.1063/1.1352596.
[56] D. Shepard, A two-dimensional interpolation function for irregularly-spaced data, in: Proceedings of the 1968 23rd ACM National Conference, New York, United States, August 27-29, 1968.
[57] R. Franke, G. Nielson, Smooth interpolation of large sets of scattered data, Int. J. Numer. Methods Eng. 15 (1980) 1691–1704, https://doi.org/10.1002/nme.1620151110.
[58] Y.U. Nam, K.D. Lee, A 280 GHz single-channel millimeter-wave interferometer system for KSTAR, Rev. Sci. Instrum. 79 (2008), 10E705, https://doi.org/10.1063/1.2957924.
[59] H.K. Na, S. Sajjad, J.M. Park, M. Kwon, Configuration and installation design of optical diagnostic systems on KSTAR, Fusion Eng. Des. 86 (2011) 66–70, https://doi.org/10.1016/j.fusengdes.2010.08.014.
[60] E. Doyle, R. Groebner, K. Burrell, P. Gohil, T. Lehecka, N. Luhmann Jr., H. Matsumoto, T. Osborne, W. Peebles, R. Philipona, Modifications in turbulence and edge electric fields at the L–H transition in the DIII-D tokamak, Phys. Fluid. Plasma Phys. 3 (1991) 2300–2307, https://doi.org/10.1063/1.859597.
[61] D. D'ippolito, J. Myra, S. Zweben, Convective transport by intermittent blob-filaments: comparison of theory and experiment, Phys. Plasmas 18 (2011), 060501, https://doi.org/10.1063/1.3594609.
[62] J. Marki, R.A. Pitts, T. Eich, A. Herrmann, J. Horacek, F. Sanchez, G. Veres, Sheath heat transmission factors on TCV, J. Nucl. Mater. 363 (2007) 382–388, https://doi.org/10.1016/j.jnucmat.2007.01.197.
[63] J.G. Bak, H.S. Kim, M.K. Bae, K.S. Chung, S.H. Hong, Study on divertor particle and heat fluxes from electric probe measurements during ELMy H-modes in KSTAR, Fusion Eng. Des. 109 (2016) 836–842, https://doi.org/10.1016/j.fusengdes.2016.01.066.